

An Evaluation of Three Distance Measurement Technologies for Flying Light Specks*

Trung Phan, Hamed Alimohammadzadeh, Heather Culbertson, Shahram Ghandeharizadeh

Computer Science Department

University of Southern California

Los Angeles, CA, USA

{taphan,halimoha,hculbert,shahram}@usc.edu

Abstract—This study evaluates the accuracy of three different types of time-of-flight sensors to measure distance. We envision the possible use of these sensors to localize swarms of flying light specks (FLSs) to illuminate objects and avatars of a metaverse. An FLS is a miniature-sized drone configured with RGB light sources. It is unable to illuminate a point cloud by itself. However, the inter-FLS relationship effect of an organizational framework will compensate for the simplicity of each individual FLS, enabling a swarm of cooperating FLSs to illuminate complex shapes and render haptic interactions. Distance between FLSs is an important criterion of the inter-FLS relationship. We consider sensors that use radio frequency (UWB), infrared light (IR), and sound (ultrasonic) to quantify this metric. Obtained results show only one sensor is able to measure distances as small as 1 cm with a high accuracy. A sensor may require a calibration process that impacts its accuracy in measuring distance.

I. INTRODUCTION

A Flying Light Speck, FLS, is a miniature sized drone configured with RGB light sources [1]–[3]. Swarms of FLS may illuminate 3D objects and avatars in the metaverse in a fixed 3D volume, an FLS display [4]. These objects may provide users with haptic feedback, both kinesthetic (force) and tactile (skin-based). Figure 1 shows FLSs illuminating the bricks of the game Jenga. As the user pushes an illuminated Jenga brick, the FLSs will push back to provide kinesthetic feedback. This force will be consistent with the surface friction between the brick and those below, above, and adjacent to it.

Both shape illuminations and kinesthetic haptic interactions require FLSs to localize. Consider each in turn. To illuminate a shape, a swarm of FLSs must preserve a pre-specified relative distance between one another. The pre-specified distance is defined by the points in a point cloud where each point is assigned to a different FLS [4]. With kinesthetic feedback, when a user pushes on a swarm of FLSs, each FLS will compute its displaced distance and the speed of its displacement. This information will be aggregated to quantify the force exerted by a user. It will enable the swarm to exhibit the appropriate behavior (e.g., bricks at the top tower falling due to excessive force applied too fast) or generate force consistent with the user’s expectation (e.g., the brick slides out gently while providing the sensation of surface resistance).

This research was supported in part by the National Science Foundation grant IIS-2232382.

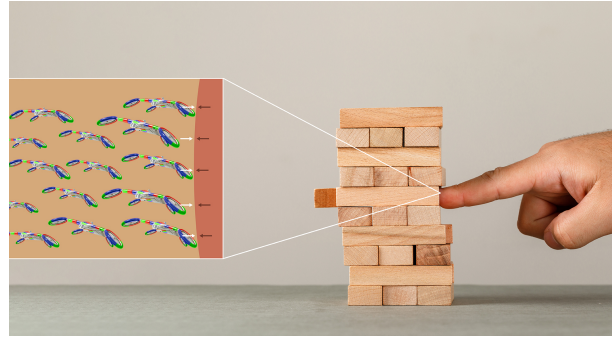


Fig. 1: FLSs rendering the game Jenga.

Measuring small distances accurately is fundamental to localizing FLSs. The ideal sensor should exhibit the following features. First, an FLS should be able to measure its distance to another FLS at a granularity that is a function of both its size and important physical parameters. A physical parameter is downwash, a region of instability caused by the flight of one FLS that adversely impacts other FLSs entering this region [5]–[10], e.g., loss of control or unpredictable behavior. FLSs must be able to measure distance at sufficient granularity to enable them to avoid each other’s downwash.

Second, the measured distances should be highly accurate. Error impacts both the quality of an illumination and how effectively FLSs render kinesthetic feedback. We define the tolerable error as a function of FLS size and important physical characteristics, e.g., 1% of the length of an FLS, 1% of the length/height/width of the downwash region.

The application requirements will also be an important factor in dictating both the granularity of measured distance and its tolerable delay. We anticipate these requirements to start simple and evolve to define next-generation devices due to the novelty of FLS displays.

In this study, we evaluate four sensors of three different technologies to measure distance between FLSs, see Table I. Our objective is to accurately measure distances as small as 1 cm. Our experiments are conducted as follows. After calibrating a sensor (if required), we place a drone a fixed distance D away from the sensor and gather its reported distances for 60 seconds. We partition these into non-overlapping windows

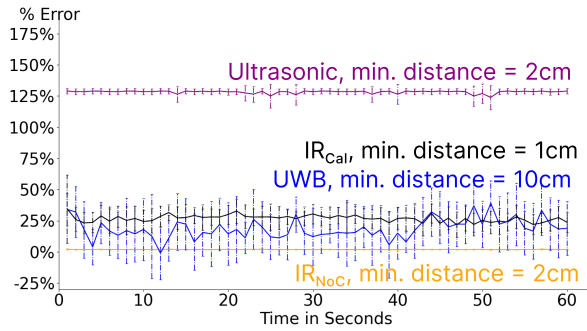


Fig. 2: A comparison of 4 sensors in measuring their minimum advertised distance. We set the minimum at 1 cm with IR_{Cal} . In these experiments, IR_{Cal} was calibrated at 1 cm and UWB was calibrated at 10 cm.

of time, each with duration δ seconds. For each window of time, we report the minimum, average, and maximum percentage error. With a window of time consisting of M samples $\{S_1, S_2, \dots, S_M\}$, we define the average percentage error as: $100 \times \frac{\sum_{i=1}^M S_i - D}{M}$.

Summary of results: In our experiments, only one infrared sensor, IR_{Cal} , is able to measure distances as small as 1 cm with approximately 10-15% error, see discussions of Figure 6b. The minimum range of UWB, IR_{NoCr} , and ultrasonic is greater than 1 cm, see Table I. Hence, they are unable to measure 1 cm accurately. Ultrasonic shows a high margin of error (125%) when measuring its minimum distance, 2 cm, see Figure 2. The margin of error is lower with UWB when measuring its minimum distance of 10 cm. However, it is still significant at 20-30%.

Both IR_{Cal} and UWB measure a distance more accurately when calibrated for that distance. Their percentage error is close to zero with distances of 20 cm and 100 cm. Ultrasonic is equally accurate with a distance of 20 cm and does not require calibration. It is possible to calibrate IR_{Cal} and UWB at one distance and measure a different distance. This increases their margin of error.

The primary **contribution** of this paper is to quantify the percentage error observed with the sensors of Table I for specific experimental setups. The rest of this paper is organized as follows. Section II presents the related research.

TABLE I: Three time-of-flight sensor types, their representatives, and advertised specifications: Ultra Wide Band (UWB) (Decawave, DW1000) [11], Infrared (IR) (SparkFun, VL53L4CD [12] and Sharp, GP2Y0A51SK0F [13]), and Ultrasonic (US) (ELEGOO, HC-SR04) [14].

	Calibrate Required	Min-Max Distance	Error	Ranging	Price/Sensor
UWB [11]	Yes	10-29K cm	≤ 10 cm	2-way	\$40
IR_{Cal} [12]	Yes	0-130 cm	≤ 0.1 cm	1-way	\$20
IR_{NoCr} [13]	No	2-15 cm	≤ 0.1 cm	1-way	\$12
US [14]	No	2-400 cm	≤ 0.3 cm	1-way	\$1.80

Sections III, IV, and V present the sensors in turn, our experimental setups, and obtained results. Brief conclusions and future works are presented in Section VI.

II. RELATED WORK

To the best of our knowledge, the quantitative analysis of the four sensors considered in this study is novel and has not been published elsewhere. Many studies have considered techniques to localize robots [15]–[17]. They have investigated environments with either the robot as the only moving object (static) or other moving objects (dynamic) [15], [18], [19]. Other studies consider simultaneous localization and mapping (SLAM) of an environment, e.g., a coal mine [15], [20], [21]. Our objective to measure distance between FLSs is similar because we want to localize FLSs relative to one another to illuminate objects and provide haptic interactions. At the same time, our environment is different along several dimensions. First, the dimensions of the 3D display volume will be known in advance and used indoors. Second, a large number of miniature-sized FLSs will cooperate in this volume, thousands if not millions. The novelty is for the FLSs to maintain a relative distance from one another (illumination) and to measure their displacement due to haptic user interactions.

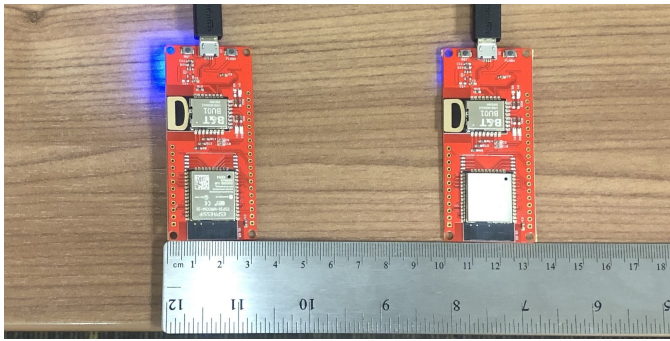
Centralized indoor techniques such as optical motion capture systems merge images from fixed cameras positioned around a display volume to localize quadrotors and drones [7], [22], [23]. These systems, e.g., Vicon, are highly accurate. They require a unique marker arrangement for each drone and have enabled control and navigation of swarms of tens of drones. It may be difficult (if not impossible) to form unique markers for more than tens of small drones measuring tens of millimeters diagonally [7]. Hence their scalability is limited. Moreover, these systems require broadcast at high frequency from a central computer to each drone [24]. This centralized communication channel is a single point of system failure. It has a latency of several (7) milliseconds [7] and its bandwidth will constrain the robustness and FLS swarm size. We envision FLSs with sensors to quantify distance in a decentralized manner.

III. ULTRA WIDE BAND, UWB

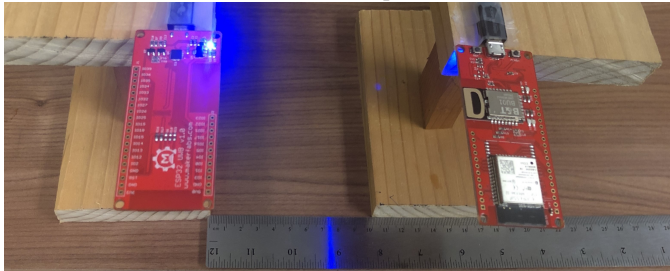
UWB is a radio frequency technology operating in a wide bandwidth [25]. Its short pulse duration enables determining the time-of-flight of the radio signal with fine granularity. Different techniques can be used for ranging and localization. With a two-way ranging technique, the distance between two devices can be measured as follows:

$$d = \frac{v_s \times (t_{rt} - t_d)}{2} \quad (1)$$

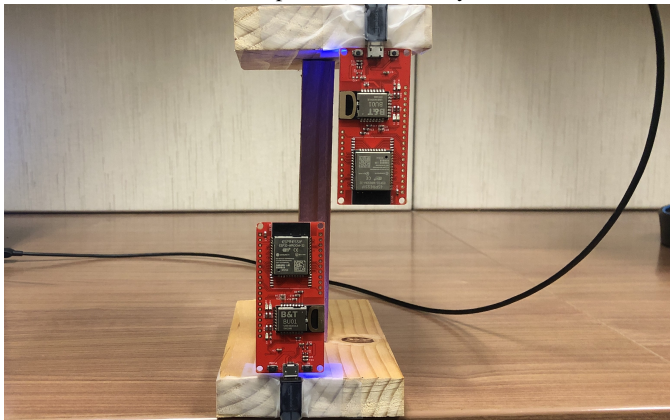
Where v_s is the speed of the radio signal, t_{rt} is the round trip time of the signal from source to destination and from the destination back to the source, and t_d is the total time spent to process the signal in the source and destination. Theoretically, UWB's short-duration pulses, in the order of nanoseconds, can provide centimeter accuracy in distance measurements [11].



(a) Tabletop.



(b) Suspended horizontally.



(c) Suspended diagonally.

Fig. 3: UWB experimental setups.

This study uses the DW1000, a single chip CMOS radio transceiver. It is compliant with the IEEE 802.15.4-1011 ultra-wideband (UWB) standard. It facilitates proximity detection to an accuracy of ± 10 cm using two-way ranging.

The provider of DW1000, Decawave, publishes a device driver for DW1000. This includes a set of APIs to initialize, configure, and measure distance using a pair of DW1000 cards. We used this software running on an Acer Swift 3 Windows laptop to make our measurements.

Figure 3 shows three alternative experimental setups for the UWB cards. The suspended cards, both horizontal and diagonal, provide the most accurate readings.

The accuracy of measured distances with UWB is impacted by its calibration process. Figure 4a shows the percentage error in measuring distance between two cards 10 cm apart. The cards were calibrated at 10, 20, and 100 cm. The percentage

error increases dramatically with higher calibrations. Figure 4b shows the percentage error in making three different distance measurements with a calibration of 10 cm. The highest percentage error is observed with a larger distance, i.e., 100 cm. If we change the calibration to 20 cm, the curve for 20 cm and 10 cm switch places, i.e., the measurements for 20 cm become more accurate. However, the measurements for 100 cm remain as inaccurate.

Figure 4c shows UWB is more accurate when calibrated for the distance it is intended to measure. Its accuracy increases with longer distances. Its average percentage error is close to 0% when measuring 100 cm distances with UWB calibrated at 100 cm.

Related Work: There are studies that use the DW1000 with anchors placed at well known coordinates to localize drones [26], [27]. Imperfect anchor clock synchronization [28] are reported as the cause of inaccuracies exceeding 7.5 cm [26]. SnapLoc [27] employs wired communication between UWB anchors to enhance localization accuracy. It reports longer distances may be measured accurately with a higher probability, e.g., 33.7 cm distances are measured accurately with a 90% probability and 60 cm distances are measured accurately with a 99% probability.

IV. INFRARED

Infrared (IR) sensors are active sensors that emit a signal (IR light) and then detect the signal's return after it bounces off of the object. The sensor calculates the distance to the object using the time-of-flight (i.e., the amount of time recorded between emitting and detecting the light):

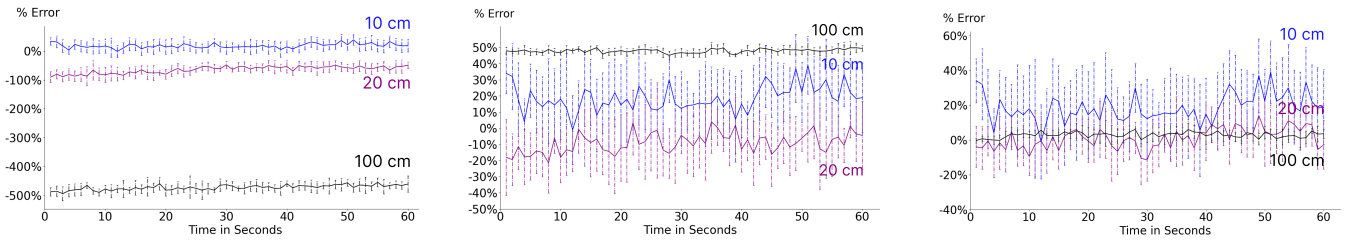
$$d = \frac{c \times t}{2} \quad (2)$$

where c is the speed of light and t is the recorded time.

IR sensors can sense closer objects and have a higher resolution than ultrasonic sensors, but they have an overall shorter range. A typical IR sensor has a range of 0–130 cm with a resolution of 1 mm [29]. However, this range can be affected by the color of the object it is detecting. While color does not change the amount of time it takes for the light to travel, lighter colors reflect more light than darker colors. Therefore, the sensor will perform optimally when detecting white objects within a specific distance range. (i.e., reflecting the most light) and its worst distance range will be when detecting black objects (i.e., reflecting the least light).

The wavelength of IR sensors (940 nm) is also significantly less than that of ultrasonic sensors, meaning that they can detect significantly smaller objects than ultrasonic sensors [29]. This parameter is very important in FLS systems. IR sensors also have a smaller FoV (18°) than ultrasonic sensors, creating a higher spatial resolution.

One limitation of IR sensors is that their performance can be affected by external light in the environment. Significant IR light from the environment can saturate the sensor or cause incorrect distance readings. Therefore, these sensors are more accurate indoors than outdoors. Best practices with IR sensors

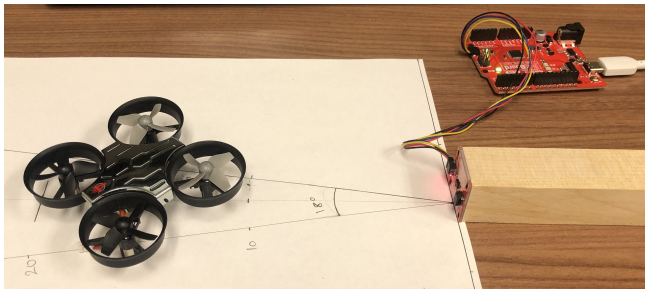


(a) Percentage error to measure 10 cm distances when calibrated at 10, 20, and 100 cm.

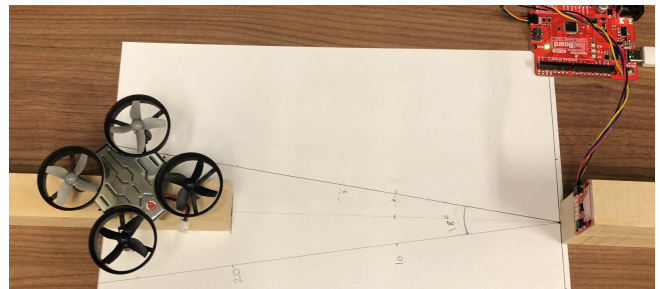
(b) Percentage error in measuring 10, 20, and 100 cm distances with a 10 cm calibration.

(c) Percentage error in measuring 10 cm with 10 cm calibration, 20 cm with 20 cm calibration, and 100 cm with 100 cm calibration.

Fig. 4: UWB quantifying different distances using alternative calibrations.



(a) IR_{Cal} sensor is touching the sheet.



(b) IR_{Cal} sensor is elevated 3.7 cm.

Fig. 5: Elevation impacts accuracy of measured distances with IR_{Cal} .

includes shielding the sensor from external light to mitigate any errors.

We evaluate the 2 IR sensors shown in Table II, the difference between them being that one requires calibration (IR_{Cal}) and the other does not (IR_{NoC}).

A. IR_{Cal} , SparkFun:VL53L4CD

With IR_{Cal} , SparkFun:VL53L4CD, we considered two experimental setups: the sensor closest to the table and the sensor raised 3.7 cm above the table. See Figure 5. Figures 6a and 6b show the accuracy of measuring different distances with a 1 cm calibration for the two setups, respectively. Note that the scale of the y-axis is logarithmic in Figure 6a. The accuracy is highest when measuring distances of 1 or 2 cm. The percentage error is higher with 10 and 20 cm. With 20 cm measurements, the elevated setup provides a lower error. Conceptually, this is due to the 3D cone shape of the sensor that is blocked by the table. We anticipate the sensors to be mounted on the FLSs and the FLSs to fly at least a few centimeters above the ground. Hence, the results of Figure 6b are most applicable.

Similar to UWB, IR_{Cal} measures a distance more accurately when it is calibrated for the distance. Figure 6c shows this and an enhanced accuracy with longer distances. The average percentage error is close to 0% with 2, 10, and 20 cm. We were not able to calibrate IR_{Cal} to measure a 100 cm distance.

B. IR_{NoC} , Sharp:GP2Y0A51SK0F

IR_{NoC} , Sharp:GP2Y0A51SK0F, does not require calibration. It is more accurate when a piece of white paper is wrapped around the cages of drone blades, compare 7a with 8a. Figures 7b and 8b show this sensor is highly accurate in measuring its minimum advertised distance of 2 cm, see Figure 7b. Its accuracy is lower when measuring longer distances and worst at its maximum of 15 cm.

V. ULTRASONIC

Similar to infrared sensing, ultrasonic sensors work by emitting a high-frequency sound that bounces off of an object and then returns to be detected by the sensor. They are a type of time-of-flight sensor, meaning that distance is calculated by measuring the amount of time that the sound takes to return to the sensor:

$$d = \frac{a \times t}{2} \quad (3)$$

where a is the speed¹ of sound and t is the recorded time. Ultrasonic sensors have a minimum and maximum distance that they can measure due to the measurement speed of the sensor and the dissipation of sound, respectively. If there are multiple objects in front of the ultrasonic sensor, the sound will bounce off the closest one, hence only the distance of the closest object will be returned. Typical ultrasonic sensors have a range of 2–400 cm with a resolution of 3 mm [30].

¹Speed of sound depends on the type of medium and the temperature of the medium. Our experiments are conducted in room temperature.

TABLE II: Two Infrared (IR) sensors. SparkFun, VL53L4CD [12], and Sharp, GP2Y0A51SK0F [13].

	Manufacturer Model Number	Calibration Required	Min-Max Distance	Error	Ranging	Price/Sensor
IR_{Cal}	SparkFun:VL53L4CD [12]	Yes	0-130 cm	≤ 0.1 cm	1-way	\$20
IR_{NoC}	Sharp:GP2Y0A51SK0F [13]	No	2-15 cm	Not Available	1-way	\$12

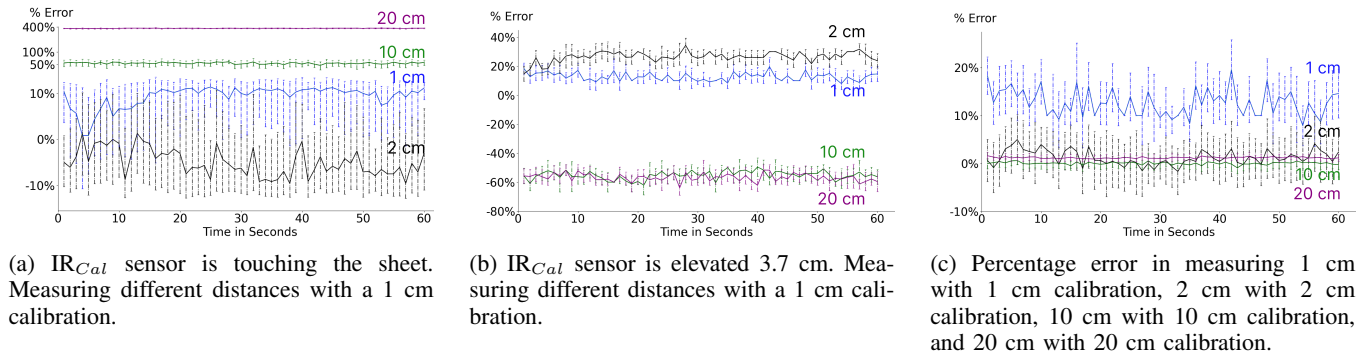
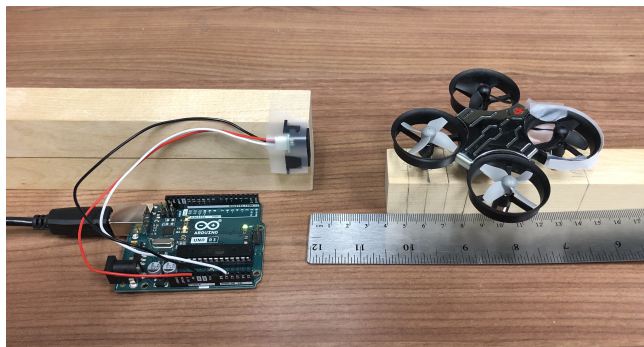
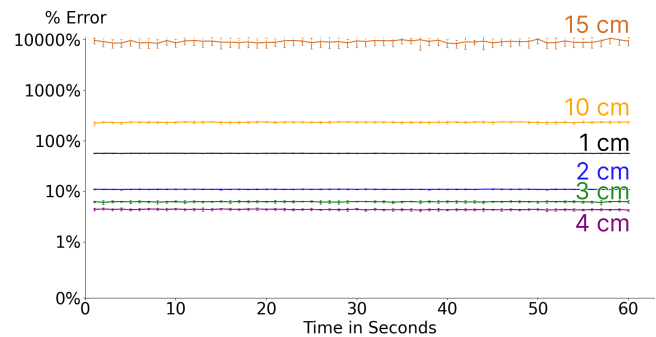


Fig. 6: IR_{Cal} quantifying different distances using alternative calibrations.

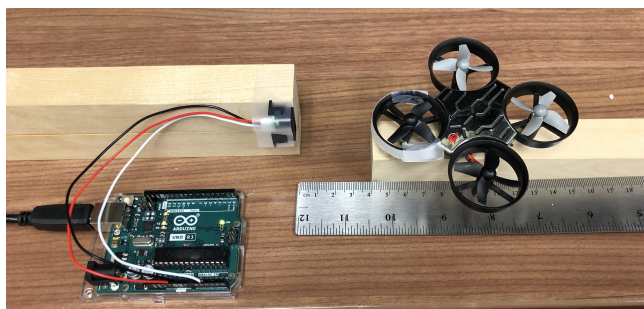


(a) IR_{NoC} Sharp:GP2Y0A51SK0F is elevated 3.7 cm.

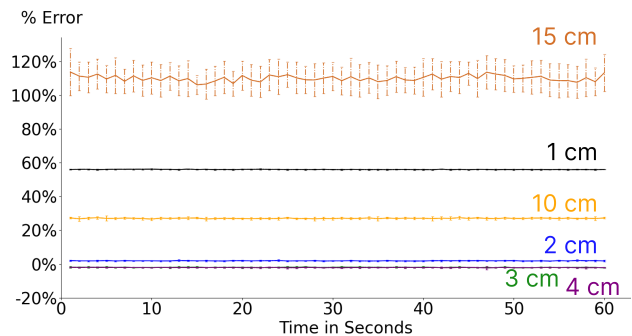


(b) Percentage error measuring different distances using the IR_{NoC} Sharp:GP2Y0A51SK0F sensor.

Fig. 7: IR_{NoC} Sharp:GP2Y0A51SK0F.

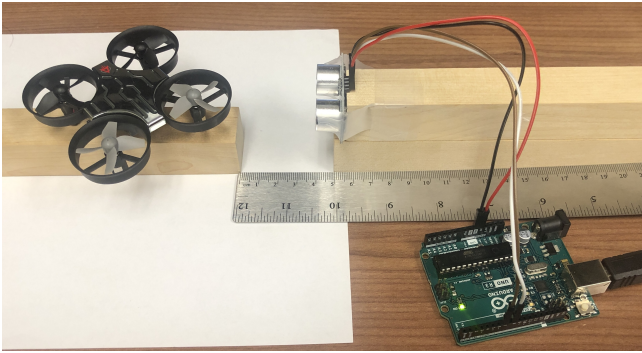


(a) IR_{NoC} Sharp:GP2Y0A51SK0F with a white piece of paper for the drone cage.

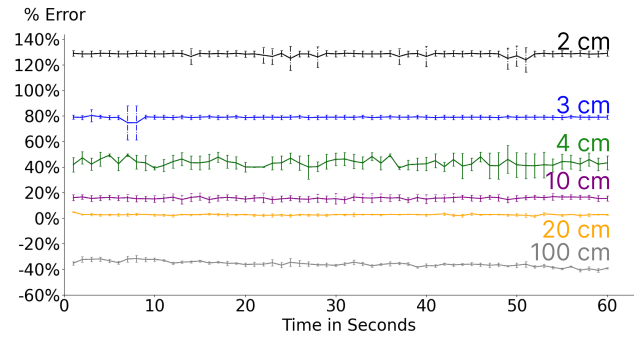


(b) Percentage error measuring different distances using the experimental setup of Figure 8a.

Fig. 8: IR_{NoC} Sharp:GP2Y0A51SK0F.



(a) Ultrasonic is elevated 3.7 cm.



(b) Percentage error measuring different distances using the ultrasonic sensor.

Fig. 9: Ultrasonic.

The size of an object that can be detected by an ultrasonic sensor is limited by the sounds' wavelength. An ultrasonic sensor that emits a 40 kHz burst of sound has a wavelength of 8.6 mm. Objects smaller than this wavelength will cause scattering of the sound, but will not cause the sound to bounce back and return to the sensor. Therefore, the sensor may not detect objects smaller than its wavelength.

The sound that is emitted from an ultrasonic sensor spreads the further it travels away from the sensor, similar to the beam of a flashlight. The cone-shaped emission of sound results in a set angular resolution for an ultrasonic sensor. This field of view (FoV) is typically around 30° , and determines the spatial resolution of an FLS. To detect FLSs in more than this limited angular area, an FLS may use (1) a single ultrasonic sensor that rotates, (2) multiple ultrasonic sensors that are oriented around the FLS, or (3) communicate with other FLSs surrounding it to gather their detected FLSs.

When using ultrasonic sensors to measure distance, it is best practice to ensure the surface properties of all objects are textured [31]. Ultrasonic sensors have a tendency towards specular reflections when looking at shiny, mirrored, or glass objects. With specular reflections, the angle of reflection is equal to the angle of incidence, meaning that the sound is less likely to return to the sensor. Thus, shiny objects may not be detected or may appear far away. These considerations are important when designing FLSs.

Since ultrasonic sensors work only by measuring the amount of time that elapses between when a sound is emitted and when it is detected, there can be issues in a system consisting of multiple FLSs using ultrasonic sensors. For example, if two FLSs are 1 m away from each other and are trying to measure that distance, if their ultrasonic sensors are pointed at each other it is likely that they could read a distance of only 0.5 m due to interference between the two sensors. Therefore, with an FLS display, more advanced signal processing and sensors would be required, such as amplitude- or frequency-modulated ultrasonic sensors.

Figure 9b shows the percentage error observed in measuring different distances with ultrasonic [14]. The experimental setup is shown in Figure 9a. The ultrasonic is most accurate

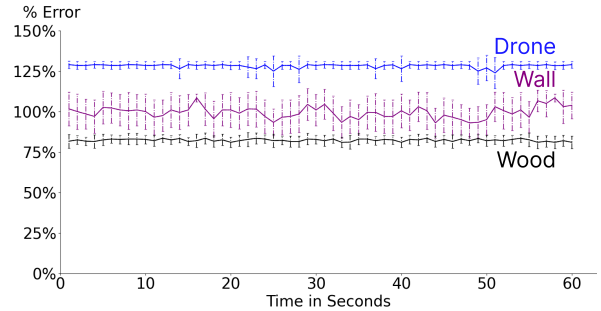


Fig. 10: Ultrasonic with different material for a target object 2 cm away.

for measuring distances of 10 and 20 cm. Its accuracy is lower with shorter (≤ 4 cm) and longer distances (≥ 100 cm).

The error observed when measuring small distances (2 cm) is sensitive to the material used by the object, see Figure 10.

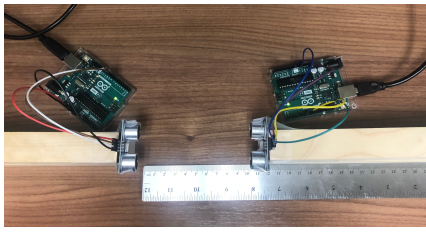
Figure 11 shows an experiment with two Ultrasonic sensors facing one another and 10 cm apart. The sensors interfere with one another with each reporting a distance of 5 cm.

Figure 12 shows the Ultrasonic sensor with two wooden square pillars in its field of view. One is 10 cm and the other is 20 cm away from the sensor. The sensor reports the distance to the closest object.

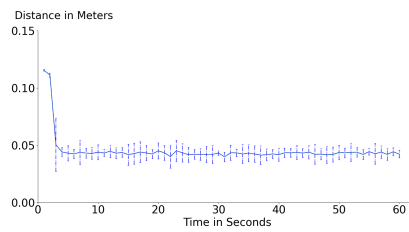
VI. CONCLUSIONS AND FUTURE RESEARCH DIRECTIONS

This paper compares several time-of-flight sensors to measure small distances. The sensors are based on different technologies: radio (UWB), light (IR), and sound (US). Only one product, *IR_{Cal}* (SparkFun:VL53L4CD), measured distances as small as 1 cm with a high accuracy. Its accuracy depends on the distance used for its calibration with a calibration of 1 cm providing the highest accuracy, 10-15%.

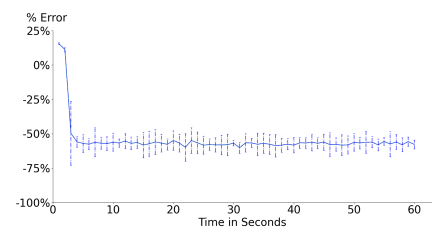
The obtained results motivate techniques that fuse measurements from different sensors to estimate distance between FLSs. Examples include Inertial-Measurement-Unit (IMU) with visual features from a camera [32]–[34], LiDAR with odometry [35]–[38], UWB with IMU and images from a camera [39]–[42], UWB with IMU and LiDAR [43].



(a) Experimental setup.

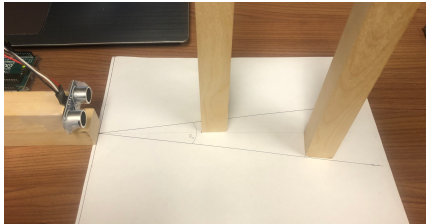


(b) Measured distance when 10 cm apart.

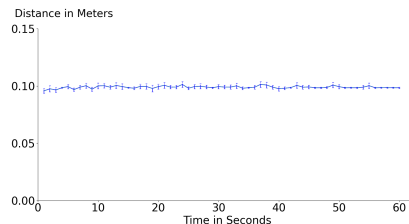


(c) A 50% error in measuring distance is anticipated with two sensors interfering with one another.

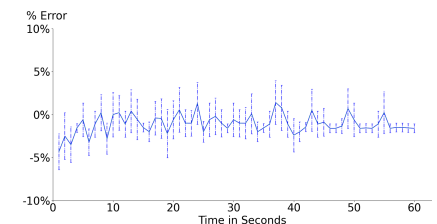
Fig. 11: Two ultrasonic sensors facing one another.



(a) Experimental setup.



(b) Sensor reports distance to the closest object.



(c) Percentage error in measuring the distance to closest object, 10cm away.

Fig. 12: Ultrasonic sensor with two objects, 10 and 20 cm away from the sensor.

We are extending this study in several directions. First, we are considering sensors that use Frequency-Modulated Continuous Wave [44] (FMCW) instead of time-of-flight. An example is radar [45]. Our objective is to identify the least expensive and most accurate sensor to measure small distances ($\leq 1\text{cm}$). We will equip FLSs with the identified sensor to design and implement localization, collision avoidance, and haptic interaction techniques. An FLS display will illuminate objects and avatars of a metaverse, enabling users to see them without wearing head mounted displays and have haptic interactions without wearing gloves.

VII. ACKNOWLEDGMENTS

This research was supported in part by the NSF grant IIS-2232382.

REFERENCES

- [1] S. Ghandeharizadeh, "Holodeck: Immersive 3D Displays Using Swarms of Flying Light Specks," in *ACM Multimedia Asia*, December 2021.
- [2] S. Ghandeharizadeh and L. Garcia, "Safety in the Emerging Holodeck Applications," in *CHI 2022 Workshop on Novel Challenges of Safety, Security and Privacy in Extended Reality*, April 2022.
- [3] H. Alimohammadzadeh, D. Mehraban, and S. Ghandeharizadeh, "Modeling Illumination Data with Flying Light Specks," in *ACM Multimedia Systems*, ser. MMSys '23. New York, NY, USA: Association for Computing Machinery, 2023.
- [4] S. Ghandeharizadeh, "Display of 3D Illuminations using Flying Light Specks," in *ACM Multimedia*, ser. MM '22. New York, NY, USA: Association for Computing Machinery, 2022.
- [5] J. van den Berg, D. Wilkie, S. Guy, M. Niethammer, and D. Manocha, "LQG-obstacles: Feedback Control with Collision Avoidance for Mobile Robots with Motion and Sensing Uncertainty," in *Proceedings - IEEE International Conference on Robotics and Automation*. IEEE, 05 2012, pp. 346–353.
- [6] S. H. Arul and D. Manocha, "DCAD: Decentralized Collision Avoidance With Dynamics Constraints for Agile Quadrotor Swarms," *IEEE Robotics and Automation Letters*, vol. 5, pp. 1191–1198, 2020.
- [7] J. Preiss, W. Honig, G. Sukhatme, and N. Ayanian, "Crazyswarm: A Large Nano-Quadcopter Swarm," in *IEEE International Conference on Robotics and Automation (ICRA)*, 05 2017, pp. 3299–3304.
- [8] D. Bareiss and J. van den Berg, "Reciprocal Collision Avoidance for Robots with Linear Dynamics using LQR-Obstacles," in *Proceedings - IEEE International Conference on Robotics and Automation*, 05 2013, pp. 3847–3853.
- [9] E. Ferrera, A. Alcántara, J. Capitán, Á. R. Castaño, P. Marrón, and A. Ollero, "Decentralized 3D Collision Avoidance for Multiple UAVs in Outdoor Environments," *Sensors (Basel, Switzerland)*, vol. 18, 2018.
- [10] Y. Xu, S. Lai, J. Li, D. Luo, and Y. You, "Concurrent Optimal Trajectory Planning for Indoor Quadrotor Formation Switching," *Journal of Intelligent & Robotic Systems*, vol. 94, 05 2019.
- [11] Decawave, "DW1000 User Manual: How to Use, Configure, and Program the DW1000 UWB Transceiver. See <https://www.qorvo.com/products/da007967>," 2017.
- [12] S. life.augmented, "VL53L4CD Datasheet. See <https://cdn.sparkfun.com/assets/d/b/b/7/c/vl53l4cd.pdf>," 2022.
- [13] Sharp, "GP2Y0A51SK0F Distance Measuring Sensor Unit. See https://global.sharp/products/device/lineup/data/pdf/datasheet/gp2y0a51sk_e.pdf."
- [14] E. Freaks, "Ultrasonic Ranging Module HC - SR04. See <https://cdn.sparkfun.com/datasheets/Sensors/Proximity/HCSR04.pdf>."
- [15] U. Wong, A. Morris, C. Lea, J. Lee, C. Whittaker, B. Garney, and R. Whittaker, "Comparative Evaluation of Range Sensing technologies for Underground Void Modeling," in *IEEE/RSJ International Conference on Intelligent Robots and Systems*, 2011, pp. 3816–3823.
- [16] P. Panigrahi and S. Bisoy, "Localization Strategies for Autonomous Mobile Robots: A review," *Journal of King Saud University - Computer and Information Sciences*, vol. 34, 03 2021.
- [17] B. Amjad, Q. Z. Ahmed, P. I. Lazaridis, M. Hafeez, F. A. Khan, and Z. D. Zaharis, "Radio SLAM: A Review on Radio-Based Simultaneous Localization and Mapping," *IEEE Access*, vol. 11, pp. 9260–9278, 2023.
- [18] C. Yuan, Y. Xu, and Q. Zhou, "PLDS-SLAM: Point and Line Features SLAM in Dynamic Environment," *Remote Sensing*, vol. 15, no. 7, 2023. [Online]. Available: <https://www.mdpi.com/2072-4292/15/7/1893>
- [19] R. G. Goswami, P. V. Amith, J. Hari, A. Dhaygude, P. Krishnamurthy,

- J. Rizzo, A. Tzes, and F. Khorrami, "Efficient Real-Time Localization in Prior Indoor Maps Using Semantic SLAM," in *2023 9th International Conference on Automation, Robotics and Applications (ICARA)*, 2023, pp. 299–303.
- [20] J. Wynne, T. Titus, A. Agha-Mohammadi, A. Azua, P. Boston, P. De León, C. Demirel-Floyd, J. De Waele, H. Jones, M. Malaska, A. Miller, H. Sapers, F. Sauro, D. Sonderegger, K. Uckert, U. Wong, E. Alexander, Jr, L. Chiao, G. Cushing, and K. Williams, "Fundamental Science and Engineering Questions in Planetary Cave Exploration," *The Journal of Geophysical Research Planets*, vol. 127, p. e2022JE007194, 11 2022.
- [21] S. Kumar Singh, B. Pratap Banerjee, and S. Raval, "A Review of Laser Scanning for Geological and Geotechnical Applications in Underground Mining," *International Journal of Mining Science and Technology*, vol. 33, no. 2, pp. 133–154, 2023. [Online]. Available: <https://www.sciencedirect.com/science/article/pii/S2095268622001409>
- [22] A. Kushleyev, D. Mellinger, C. Powers, and V. Kumar, "Towards a Swarm of Agile Micro Quadrotors," *Autonomous Robots*, vol. 35, pp. 573–7527, 11 2013.
- [23] R. Ritz, M. W. Müller, M. Hehn, and R. D'Andrea, "Cooperative Quadcopter Ball Throwing and Catching," in *2012 IEEE/RSJ International Conference on Intelligent Robots and Systems*, 2012, pp. 4972–4978.
- [24] A. Weinstein, A. Cho, G. Loianno, and V. Kumar, "Visual Inertial Odometry Swarm: An Autonomous Swarm of Vision-Based Quadrotors," *IEEE Robotics and Automation Letters*, vol. 3, no. 3, pp. 1801–1807, 2018.
- [25] K. Siwiak, "Ultra-wide Band Radio: Introducing a New Technology," in *IEEE VTS 53rd Vehicular Technology Conference, Spring 2001. Proceedings (Cat. No.01CH37202)*, vol. 2, 2001, pp. 1088–1093 vol.2.
- [26] A. Ledergerber, M. Hamer, and R. D'Andrea, "A Robot Self-Localization System using One-Way Ultra-Wideband Communication," in *2015 IEEE/RSJ International Conference on Intelligent Robots and Systems (IROS)*, 2015, pp. 3131–3137.
- [27] B. GroBwindhager, M. Stocker, M. Rath, C. A. Boano, and K. Römer, "SnapLoc: An Ultra-Fast UWB-Based Indoor Localization System for an Unlimited Number of Tags," in *ACM/IEEE International Conference on Information Processing in Sensor Networks (IPSN)*, no. 18, 2019, pp. 61–72.
- [28] H. Chen and A. Dhekne, "A Metric for Quantifying UWB Ranging Error Due to Clock Drifts," in *2022 IEEE 12th International Conference on Indoor Positioning and Indoor Navigation (IPIN)*, 2022, pp. 1–8.
- [29] G. Benet, F. Blanes, J. E. Simó, and P. Pérez, "Using Infrared Sensors for Distance Measurement in Mobile Robots," *Robotics and Autonomous Systems*, vol. 40, no. 4, pp. 255–266, 2002.
- [30] T. Mohammad, "Using Ultrasonic and Infrared Sensors for Distance Measurement," *World Academy of Science, Engineering and Technology*, vol. 51, pp. 293–299, 2009.
- [31] L. Kleeman and R. Kuc, *Sonar Sensing*. Berlin, Heidelberg: Springer Berlin Heidelberg, 2008, pp. 491–519.
- [32] R. Mur-Artal and J. D. Tardós, "ORB-SLAM2: An Open-Source SLAM System for Monocular, Stereo, and RGB-D Cameras," *IEEE Transactions on Robotics*, vol. 33, no. 5, pp. 1255–1262, 2017.
- [33] T. Qin, P. Li, and S. Shen, "VINS-Mono: A Robust and Versatile Monocular Visual-Inertial State Estimator," *IEEE Transactions on Robotics*, vol. 34, no. 4, pp. 1004–1020, 2018.
- [34] P. Geneva, K. Eickenhoff, W. Lee, Y. Yang, and G. Huang, "OpenVINS: A Research Platform for Visual-Inertial Estimation," in *Proc. of the IEEE International Conference on Robotics and Automation*, Paris, France, 2020. [Online]. Available: https://github.com/rpng/open_vins
- [35] R. Dube, A. Gawel, H. Sommer, J. Nieto, R. Siegwart, and C. Cadena, "An online multi-robot SLAM system for 3D LiDARs," in *Proc. IEEE/RSJ International Conference on Intelligent Robots and Systems*, 09 2017, pp. 1004–1011.
- [36] J. Zhang and S. Singh, "LOAM: Lidar Odometry and Mapping in Real-time," in *Robotics: Science and Systems X, University of California, Berkeley, USA, July 12-16, 2014*, D. Fox, L. E. Kavraki, and H. Kurniawati, Eds., 2014. [Online]. Available: <http://www.roboticsproceedings.org/rss10/p07.html>
- [37] H. Wang, C. Wang, C.-L. Chen, and L. Xie, "F-LOAM: Fast LiDAR Odometry and Mapping," in *2021 IEEE/RSJ International Conference on Intelligent Robots and Systems (IROS)*. IEEE Press, 2021, p. 4390–4396. [Online]. Available: <https://doi.org/10.1109/IROS51168.2021.9636655>
- [38] J. Lin and F. Zhang, "Loam livox: A fast, robust, high-precision LiDAR odometry and mapping package for LiDARs of small FoV," in *2020 IEEE International Conference on Robotics and Automation (ICRA)*, 2020, pp. 3126–3131.
- [39] H. Xu, L. Wang, Y. Zhang, K. Qiu, and S. Shen, "Decentralized Visual-Inertial-UWB Fusion for Relative State Estimation of Aerial Swarm," in *2020 IEEE International Conference on Robotics and Automation (ICRA)*, 2020, pp. 8776–8782.
- [40] H. Xu, Y. Zhang, B. Zhou, L. Wang, X. Yao, G. Meng, and S. Shen, "Omni-Swarm: A Decentralized Omnidirectional Visual-Inertial-UWB State Estimation System for Aerial Swarms," *IEEE Trans. Robotics*, vol. 38, no. 6, pp. 3374–3394, 2022. [Online]. Available: <https://doi.org/10.1109/TRO.2022.3182503>
- [41] P.-Y. Kao, H.-J. Chang, K.-W. Tseng, T. Chen, H.-L. Luo, and Y.-P. Hung, "VIUNet: Deep Visual-Inertial-UWB Fusion for Indoor UAV Localization," *IEEE Access*, vol. 11, pp. 61 525–61 534, 2023.
- [42] B. Yang, J. Li, and H. Zhang, "Resilient Indoor Localization System Based on UWB and Visual-Inertial Sensors for Complex Environments," *IEEE Transactions on Instrumentation and Measurement*, vol. 70, pp. 1–14, 2021.
- [43] T.-M. Nguyen, M. Cao, S. Yuan, Y. Lyu, T. H. Nguyen, and L. Xie, "LIRO: Tightly Coupled Lidar-Inertia-Ranging Odometry," in *IEEE International Conference on Robotics and Automation (ICRA)*, 2021, pp. 14 484–14 490.
- [44] N. Pohl, T. Jaschke, S. Scherr, S. Ayhan, M. Pauli, T. Zwick, and T. Musch, "Radar Measurements with Micrometer Accuracy and Nanometer stability using an Ultra-Wideband 80 GHz Radar System," in *IEEE Topical Conference on Wireless Sensors and Sensor Networks (WiSNet)*, 2013, pp. 31–33.
- [45] N. Pohl, T. Jaeschke, S. Küppers, C. Bredendiek, and D. Nüßler, "A Compact Ultra-Wideband mmWave Radar Sensor at 80 GHz based on a SiGe Transceiver Chip," in *International Microwave and Radar Conference (MIKON)*, 2018, pp. 345–347.